The Role of Poleward-Intensifying Winds on Southern Ocean Warming

JOHN C. FYFE AND OLEG A. SAENKO

Canadian Centre for Climate Modelling and Analysis, Environment Canada, Victoria, British Columbia, Canada

KIRSTEN ZICKFELD, MICHAEL EBY, AND ANDREW J. WEAVER

School of Earth and Ocean Sciences, University of Victoria, Victoria, British Columbia, Canada

(Manuscript received 8 November 2006, in final form 9 March 2007)

ABSTRACT

Recent analyses of the latest series of climate model simulations suggest that increasing CO_2 emissions in the atmosphere are partly responsible for (i) the observed poleward shifting and strengthening of the Southern Hemisphere subpolar westerlies (in association with shifting of the southern annular mode toward a higher index state), and (ii) the observed warming of the subsurface Southern Ocean. Here the role that poleward-intensifying westerlies play in subsurface Southern Ocean warming is explored. To this end a climate model of intermediate complexity was driven separately, and in combination with, time-varying CO_2 emissions and time-varying surface winds (derived from the fully coupled climate model simulations mentioned above). Experiments suggest that the combination of the direct radiative effect of CO_2 emissions and poleward-intensified winds sets the overall magnitude of Southern Ocean warming, and that the poleward-intensified winds are key in terms of determining its latitudinal structure. In particular, changes in wind stress curl associated with poleward-intensified winds significantly enhance pure CO_2-induced subsurface warming around 45°S (through increased downwelling of warm surface water), reduces it at higher latitudes (through increased upwelling of cold deep water), and reduces it at lower latitudes (through decreased downwelling of warm surface water). Experiments also support recent high-resolution ocean model experiments suggesting that enhanced mesoscale eddy activity associated with poleward-intensified winds influences subsurface (and surface) warming. In particular, it is found that increased poleward heat transport associated with increased mesoscale eddy activity enhances the warming south of the Antarctic Circumpolar Current. Finally, a mechanism involving offshore Ekman sea ice transport (modulated by enhanced mesoscale activity) that acts to significantly limit the human-induced high-latitude Southern Hemisphere surface temperature response is reported on.

1. Introduction

The higher-than-expected warming of intermediate-level waters in the Southern Ocean in recent decades (Gille 2002) has been reproduced in the latest series of global climate model simulations, which include time-varying changes in anthropogenic greenhouse gases, sulfate aerosols, and volcanic aerosols in the earth's atmosphere (Fyfe 2006). The agreement between observations and state-of-the-art global climate models suggests significant human influence on Southern Ocean temperatures. Global climate model simulations also show human-induced strengthening and poleward shifting of surface wind stress (e.g., Kushner et al. 2001; Yin 2005; Fyfe and Saenko 2006), which appears to be consistent with the observed shifting of the southern annular mode (SAM) toward a higher index state (Thompson et al. 2000; Marshall 2003). The aim of this paper is to quantify the role that poleward-intensifying surface wind stress (and by association the shifting SAM index) plays in setting the warming structure of the subsurface waters in the Southern Ocean. In this investigation we focus on increasing greenhouse gases as the forcing agent but are mindful of the possibility that ozone depletion over the Antarctic may be important in the spring and summer seasons (Gillett and Thompson 2003).

Our approach is to drive a global climate model of intermediate complexity with (i) anthropogenic greenhouse gas emissions observed from 1850 to 1990 and then following the Intergovernmental Panel on Climate

Corresponding author address: Dr. J. C. Fyfe, Canadian Centre for Climate Modelling and Analysis, University of Victoria, P.O. Box 1700, Victoria, BC V8W 2Y2, Canada.
E-mail: John.Fyfe@ec.gc.ca

DOI: 10.1175/2007JCLI1764.1

Change (IPCC) Special Report on Emissions Scenarios (SRES) A2 scenario to 2100 and/or (ii) time-varying Southern Hemisphere (only) surface wind stress fields derived from the latest series of fully coupled global climate model simulations (Fyfe and Saenko 2006). In this way we will isolate and quantify the involvement of poleward-intensified winds on the evolution of subsurface Southern Ocean temperature structure. We will conclude that poleward-intensified winds have played (and will likely continue to play) a significant role in determining the warming structure of the subsurface Southern Ocean waters. Additionally, we will address a recent issue raised with respect to the importance of increasing mesoscale eddy activity (associated with increasing winds) in affecting the subsurface Southern Ocean warming (Meredith and Hogg 2006). Finally, we will report on a mechanism involving offshore Ekman sea ice transport (modulated by enhanced mesoscale activity), which acts to significantly limit the high-latitude surface temperature response.

2. Methods

a. Earth system model

In this study we use version 2.8 of the University of Victoria Earth System Climate Model (UVic ESCM) (Weaver et al. 2001). This version of the UVic ESCM consists of a three-dimensional ocean general circulation model coupled to a thermodynamic–dynamic sea ice model, an energy–moisture balance atmospheric model with dynamical feedbacks, a single-layer land surface model, and a dynamic vegetation model. The model is global in coverage and has a resolution of 3.6° (zonal) and 1.8° (meridional). Ice and snow albedo feedbacks are included in the coupled model by locally changing the surface albedo. The atmospheric model includes a parameterization of water vapor–planetary longwave feedbacks, and the radiative forcing associated with changes in atmospheric CO_2 is included as a modification of planetary long-wave flux. The dynamic global vegetation model Top-down Representation of Interactive Foliage and Flora Including Dynamics (TRIFFID; Cox 2001), together with a single soil-layer version of the Met Office Surface Exchange Scheme (MOSES) land surface scheme (Cox et al. 1998; Meissner et al. 2003), were included in the coupled model. In addition, version 2.8 of the UVic ESCM includes a terrestrial (Matthews et al. 2004) and oceanic (Schmittner et al. 2005) carbon cycle. [In a separate paper we address the role of poleward-intensified winds on the global carbon cycle (Zickfeld et al. 2007)]. In the UVic ESCM model, as in most other coarse-resolution climate models, oceanic mesoscale eddies are parameterized using the Gent and McWilliams (1990) mixing scheme with a constant coefficient of eddy isopycnal thickness diffusivity, κ. In its standard configuration (version 2.8) the UVic ESCM has $\kappa = 800\ \mathrm{m^2\ s^{-1}}$.

In the control (CNTL) configuration the UVic ESCM was run for several thousand years to near equilibrium using fixed present-day CO_2 concentration and observed monthly surface wind stress climatology. Figure 1 compares the observed and CNTL simulated time-mean and zonal-mean potential temperature structure in the Southern Ocean. A tongue of maximum cold bias (~1.5°C) extends from about 500 m at 20°S to near the surface at about 45°S. Below this region the model exhibits a small warm bias (~0.25°C). We note that these errors are very similar in magnitude and pattern to those found in the IPCC Fourth Assessment Report (AR4) model simulations (R. Stouffer 2006, personal communication) and are acceptable within the context of the present study. These errors are thought to be partly related to problems in the formation of Antarctic Intermediate Water (AAIW).

Three multicentury transient experiments of the UVic ESCM were conducted under the following configurations: 1) Time-varying CO_2 emissions (i.e., historical from 1850 to 1990 then following the IPCC SRES-A2 emissions scenario to 2100) and monthly surface wind stress climatology (as in the CNTL simulation). This is denoted the GHG experiment. 2) Fixed present-day CO_2 concentration (as in the CNTL simulation) and time-varying monthly Southern Hemisphere surface wind stress derived from an ensemble of fully coupled global climate model simulations as described below. This is denoted the Wind experiment. 3) Time-varying CO_2 emissions (as in the GHG experiment) and time-varying monthly surface wind stress (as in the Wind experiment). This is denoted the Both experiment. We have also conducted two additional experiments motivated by the concern that while a constant value of eddy thickness diffusivity, κ, may capture the effect of eddies under unperturbed climate conditions, it is unclear if keeping κ constant captures the eddy response to changing surface wind stress forcing.

Before proceeding, we note an earlier study by Oke and England (2004) who employed an ocean-only model to investigate some effects of poleward shifting of the subpolar westerlies in the Southern Hemisphere. That study generally concluded that latitudinal shifts of the westerlies may play an important role in generating temperature fluctuations at intermediate water depths.

b. Wind stress forcing

The time-varying surface wind stress fields used in this study blend the observed climatology used in the

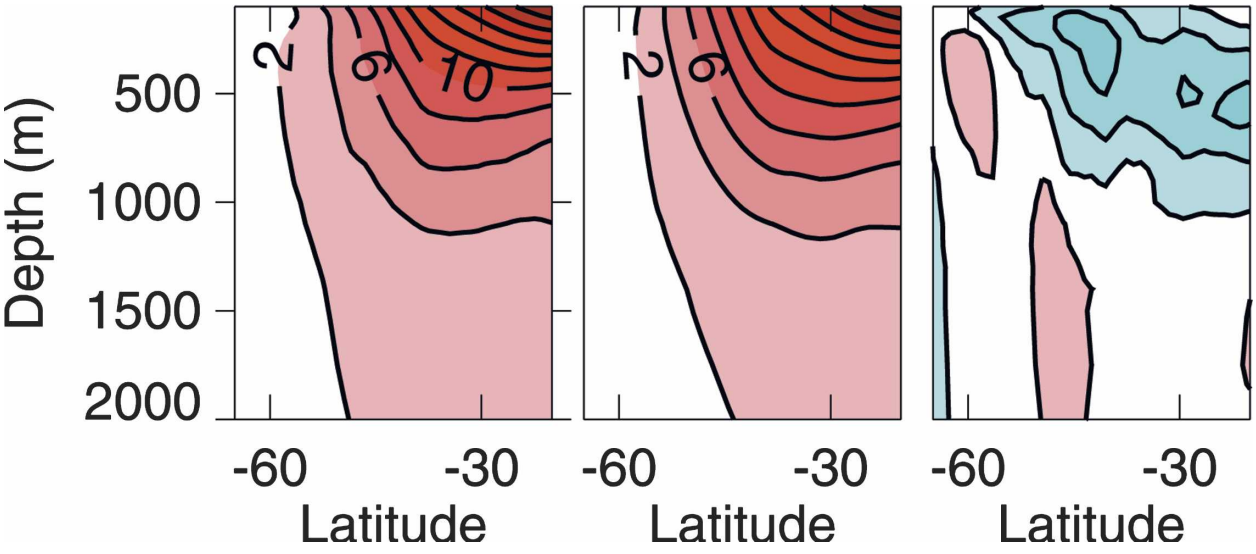

FIG. 1. Time-mean and zonal-mean (left) observed and (middle) modeled potential temperature. The observations are from the 2004 *World Ocean Atlas* (*WOA-2004*) compiled by Levitus et al. (2005) for the period 1957–90. The model results are for the CNTL simulation of the UVic ESCM. The contour interval is 2°C (2, 4, 6, . . .). (right) Model error with contour interval 0.5°C (. . . , −0.25, 0.25, 0.75, 1.25, . . .).

CNTL simulation and anomalies (for the Southern Hemisphere only) derived from the latest series of fully coupled global climate model simulations performed in support of the IPCC AR4. The climate models, which are documented at http://www-pcmdi.llnl.gov, have the following official model names: CCCMA-CGCM3.1 (Canadian Centre for Climate Modelling and Analysis Coupled General Circulation Model, version 3.1), GFDL-CM2.0 (Geophysical Fluid Dynamics Laboratory Climate Model version 2.0), GFDL-CM2.1 (version 2.1), INM-CM3.0 (Institute of Numerical Mathematics Coupled Model, version 3.0), MIROC3.2(medres) (Model for Interdisciplinary Research on Climate 3.2, medium-resolution version), MRI CGCM2.3.2a (Meteorological Research Institute Coupled General Circulation Model, version 2.3.2a), CNRM-CM3 (Centre National de Recherches Météorologiques Coupled Global Climate Model, version 3), IPSL-CM4 (L'Institut Pierre-Simon Laplace Coupled Model, version 4), MIUBECHOG (Meteorological Institute of the University of Bonn, ECHO-G Model), and MPI-ECHAM5 (Max Planck Institute ECHAM5). Surface wind stress fields were assembled from a concatenation of each model's preindustrial control run, twentieth-century run (with historical GHG, aerosol, and, in some cases, volcanic and solar forcing) and twenty-first-century run following the IPCC SRES-A2 emissions scenario. Model-mean anomalies relative to 1850 were computed, temporally smoothed (with a fourth-order polynomial in time), corrected for a small equatorward bias (Fyfe and Saenko 2006; Russell et al. 2006), and then added to the observed climatology.

Figure 2 shows the IPCC AR4 model-mean change in annual-mean wind stress maximum strength and position from 1850 to 2100. As a group, the models predict about a 25% strength increase and 3.5° poleward shift from 1850 to 2100. (Take note that the smoothness of these curves arises from application of the fourth-order polynomial in time mentioned above.) Importantly, the poleward-intensified winds are statistically significant over the period of rapid Southern Ocean warming (Gille 2002) in that the shaded regions do not overlap the zero lines during this period. Figure 3 shows the monthly variation in maximum strength and position change over time. We see that during the twentieth century the surface zonal wind stress poleward intensifies about equally (and statistically significantly) in each month of the year. During the twenty-first century the strength and position response becomes much more seasonal, for example, being the most intensified in May and the least shifted in September. The potential link between this seasonal pattern of zonal wind response and the semiannual oscillation (SAO) warrants further investigation.

We now ask how the UVic ESCM Southern Ocean temperatures respond to these surface wind stress changes in the presence and absence of time-varying CO_2 emissions. In asking this question we should keep in mind that the imposed wind stress changes are themselves the consequence of increasing CO_2 concentra-

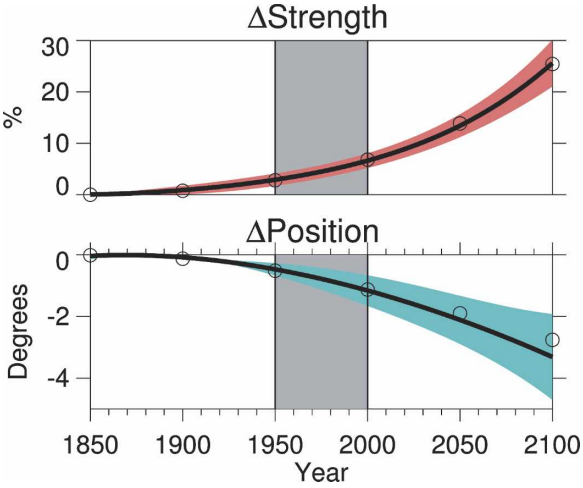

FIG. 2. IPCC AR4 model simulations showing the change in maximum Southern Hemisphere annual-mean and zonal-mean zonal surface wind stress (top) strength and (bottom) position. The curves represent the model-mean values of strength and position. The shading surrounding the curves represents the 2σ sampling variability between the models. The open dots represent the strength and position of the model-mean surface wind stress (i.e., as opposed to the model-mean strength and position). As a group the IPCC models predict about a 25% strength increase and 3.5° poleward shift of the wind stress by 2100. Importantly, there is a statistically significant poleward intensification of the winds over the period of rapid Southern Ocean warming (i.e., 1950–2000; gray shading). Take note that the smoothness of the curves arises from the application of a fourth-order polynomial in time.

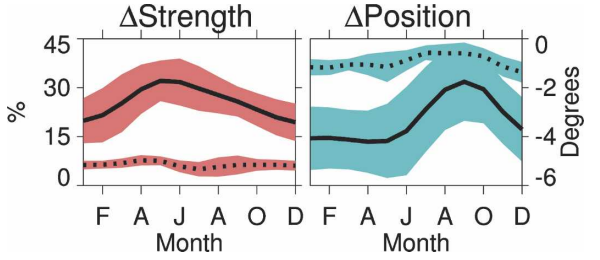

FIG. 3. IPCC AR4 model simulations showing the change in maximum Southern Hemisphere monthly mean and zonal-mean zonal surface wind stress (left) strength and (right) position. The dashed curves represent the change from 1850 to 2000. The solid curves represent the change from 1850 to 2100. The shading represents the 2σ sampling variability between the models. During the twenty-first century the strength and position response becomes very seasonal, e.g., being the most intensified in May and the least shifted in September.

tion, and that the purpose of this study is to assess the direct impact of CO_2-induced surface wind stress change on Southern Ocean warming.

3. Results

a. Simulated historical change

Figure 4 (left panel) shows the 1950 to 2000 linear trend pattern of annual- and zonal-mean ocean temperature in the UVic ESCM under the influence of both time-varying CO_2 emissions and time-varying surface wind stress, ΔT_{Both}. We see warming throughout most of the domain, with the strongest penetration of the surface signal into the deeper ocean around 43°S (shown by the dotted line). This result is in good qualitative agreement with the pattern of warming simulated in the IPCC AR4 models themselves (cf. Fig. 3 from Fyfe 2006). The enhanced subsurface warming structure around 43°S is presumably set by a combination of factors, including the relatively weak stratification in this region and downward Ekman pumping. The weak stratification is associated with the formation of low potential vorticity mode waters north of the Antarctic Circumpolar Current (ACC), while the downward Ekman pumping is associated with positive wind stress curl peaking around 40°S (not shown).

Figure 4 also shows the ocean temperature response to historical CO_2 emissions alone, ΔT_{GHG} (left middle panel), and time-varying surface wind stress alone, ΔT_{Wind} (right middle panel). It is clear that neither CO_2 emissions alone (i.e., without poleward-intensified winds) nor poleward-intensified winds alone (i.e., without CO_2 emissions) can account for the overall pattern of Southern Ocean temperature change. This implies that poleward-intensified winds have played an important, but certainly not the only role in setting the pattern of Southern Ocean temperature change. In particular, poleward-intensified winds (which themselves are anthropogenically forced) act to enhance the subsurface anthropogenic warming signal in the region between 40° and 50°S and to suppress it at higher and at lower latitudes. To quantify the respective roles played by the direct radiative forcing by CO_2 emissions and poleward-intensified winds in setting the 1950 to 2000 warming pattern we consider $\Delta T_{\text{Both}} \approx \Delta T_{\text{BothL}}$, where

$$\Delta T_{\text{BothL}} = \Gamma_{\text{GHG}} \Delta T_{\text{GHG}} + \Gamma_{\text{Wind}} \Delta T_{\text{Wind}}. \qquad (1)$$

Here Γ_{GHG} and Γ_{Wind} are constant coefficients derived from a multiple linear regression analysis between the Both trend pattern, ΔT_{Both}, and the GHG and Wind trend patterns, ΔT_{GHG} and ΔT_{Wind}, respectively. Figure 4 (right panel) shows that ΔT_{BothL} is the best approximation to ΔT_{Both} when $\Gamma_{\text{GHG}} \approx 0.98$ and $\Gamma_{\text{Wind}} \approx 0.92$. Further, we note that the poleward-intensified wind pattern explains about 40% of the spatial variance of the combined pattern (both directly, and through its cross correlation with the CO_2 emissions pattern). These calculations show that the combination of the

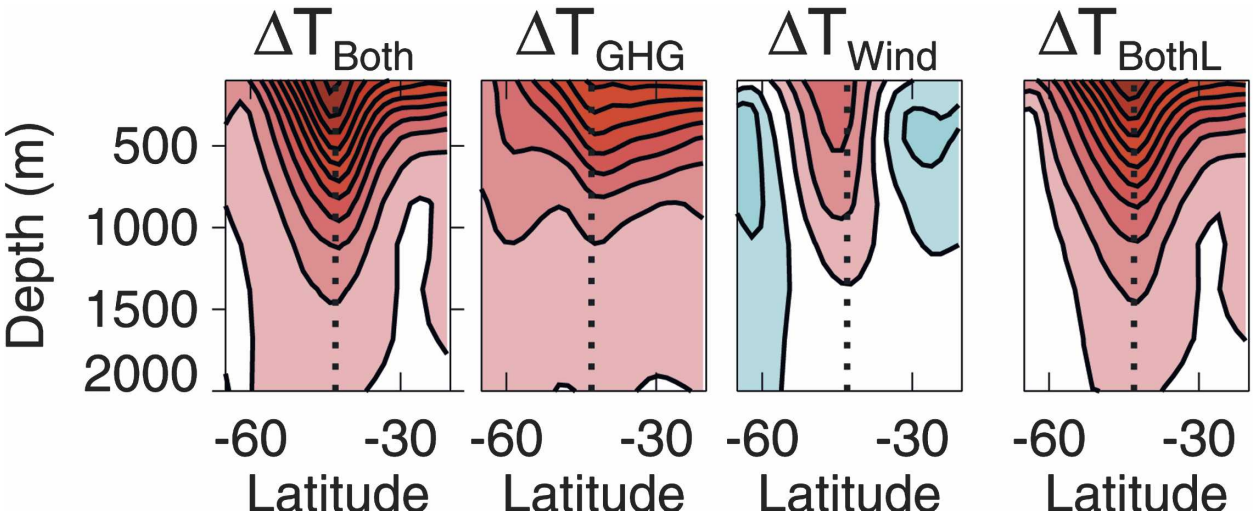

FIG. 4. UVic ESCM model simulations showing the linear trend in Southern Ocean annual-mean and zonal-mean temperature over the period from 1950 to 2000. (left) With time-varying CO_2 emissions and poleward-intensifying surface winds. (middle left) With time-varying CO_2 emissions. (middle right) With poleward-intensifying surface winds. (right) Linear combination of the CO_2 emission and poleward intensification patterns (see the text for further explanation). Contour interval is 0.0008°C yr^{-1} (. . . , −0.0004, 0.0004, 0.0012, . . .). Blue shading indicates negative values while red shading indicates positive values. Poleward-intensified winds enhance penetration of the anthropogenic warming signal in the region around 43°S.

direct radiative effect of CO_2 emissions and poleward-intensified winds sets the overall magnitude of Southern Ocean warming, and that the poleward-intensified winds are key in terms of determining its latitudinal structure. To repeat, poleward-intensified winds have played an important, but not the only, role in setting the overall subsurface warming structure since the 1950s in this model.

Stronger zonal wind stress in the Southern Ocean results in increased Ekman transport across the ACC, and hence the possibility of enhanced meridional overturning in the region. However, recent high-resolution ocean modeling results (Hallberg and Gnanadesikan 2006) suggest that increased mesoscale eddy activity can offset the effect of increased surface winds on the meridional overturning, and subsurface density structure, in the Southern Ocean. In particular, in the upper ACC the slope of isopycnals appears to be set by the competing effects of zonal surface wind stress and mesoscale eddy activity. Increased zonal wind stress tends to increase the depth of the thermocline across the ACC, whereas increased mesoscale eddy activity tends to decrease it [cf. Eq. (28) in Marshall and Radko 2003]. Thus, intensified mesoscale eddy activity in the region of the ACC, associated with the stronger winds, is expected to affect the subsurface temperature structure within the Southern Ocean (and beyond, given its connection to the rest of the World Ocean; Kamenkovich and Sarachik 2004). In particular, it has been suggested that an eddy-induced poleward heat flux may have played a significant role in the observed warming of the Southern Ocean since the 1950s (Meredith and Hogg 2006).

To assess the influence of enhanced mesoscale eddy activity on the simulated Southern Ocean warming we have conducted two additional experiments, denoted the BothE and WindE experiments. These are identical to the Both and Wind experiments except that the value of κ was transiently increased in proportion to the increase in maximum zonal-mean zonal wind stress, τ. Specifically, the change of κ through time is such that $\Delta\kappa \propto \Delta\tau$ where $\Delta\kappa = \kappa(t) - \kappa(0)$, $\Delta\tau = \tau(t) - \tau(0)$, and $\kappa(0)$ and $\tau(0)$ are year 1850 values (see the appendix for the justification of this particular approach). In these experiments, κ increases from 800 $m^2\,s^{-1}$ in 1850 to 1100 $m^2\,s^{-1}$ in 2100. We represent the direct mesoscale eddy response to poleward-intensified winds in this simple way, which nevertheless aims to plausibly capture the relevant processes. Our purpose here is to test the role of enhanced mesoscale eddy activity in the context of the Gent and McWilliams parameterization as implemented in most coarse-resolution models. It is not our purpose to propose a more suitable form for such a parameterization.

In the BothE experiment the increase in κ produces about an 8% decrease in the warming trend north of the ACC, and about a 25% increase in the warming trend south of the ACC (Fig. 5, two leftmost panels)—

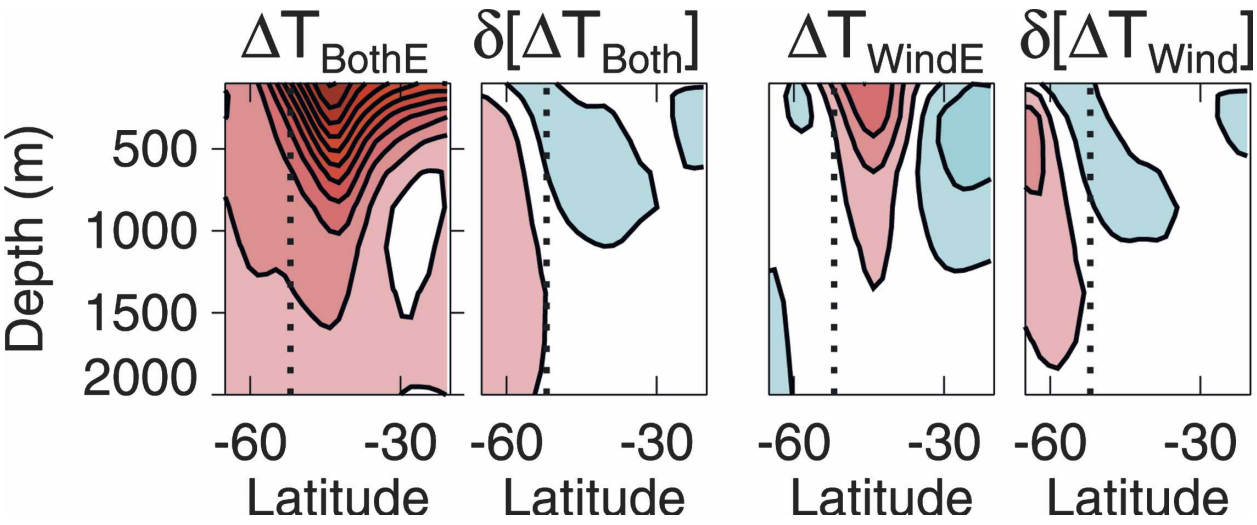

FIG. 5. UVic ESCM model simulations showing the linear trend in Southern Ocean annual-mean and zonal-mean temperature over the period from 1950 to 2000 given enhanced parameterized mesoscale eddy activity. (left) With time-varying CO_2 emissions and poleward-intensifying winds. (middle left) Difference between the BothE and Both experiments showing the effect of enhanced eddy activity in the Both simulation. (middle right) With poleward-intensifying winds only. (right) Difference between the WindE and Wind experiments showing the effect of enhanced eddy activity in the Wind simulation. Contour interval is 0.0008°C yr^{-1} (. . . , −0.0004, 0.0004, 0.0012, . . .). Blue shading indicates negative values while red shading indicates positive values. The vertical dotted line denotes the mean position of the Antarctic Circumpolar Current.

which is consistent with enhanced poleward heat flux across the ACC, as seen in recent high-resolution ocean model simulations (Meredith and Hogg 2006). These eddy-induced changes are related to increased eddy activity tending to flatten the isotherms across the ACC, thereby countering the tendency for increased winds to deepen and elevate the isotherms just north and just south of the ACC, respectively. In addition, in the region well north of the ACC (e.g., north of 40°S) the subsurface temperature structure is implicitly affected by the slope of isotherms across the ACC (Kamenkovich and Sarachik 2004). Thus, the tendency for subsurface cooling set in the subtropics by a positive Ekman pumping anomaly (see Fig. 7, and the relevant discussion in the next subsection) becomes more pronounced with increased mesoscale eddy activity.

We now turn to UVic ESCM projections for the twenty-first century.

b. Simulated projected change

Figure 6 shows the projected change to year 2100 in the depth-integrated water temperature for the various experiments. As can be seen, the poleward-intensified winds play an important role in setting the overall structure of the projected Southern Ocean warming, that is, by enhancing the direct CO_2-induced warming around 45°S, and inhibiting it to the north and south. Also, as suggested in a previous study with a high-resolution ocean model (Meredith and Hogg 2006), enhanced mesoscale eddy activity contributes quite significantly to the Southern Ocean warming south of the ACC (e.g., leading to about a 25% increase in the warming south of the ACC). An important implication here is that the IPCC AR4 models that do not adequately account for increased eddy activity associated with strengthened winds may be underestimating warming south of the ACC.

Much of the Southern Ocean warming structure is readily explained by the corresponding changes in Ekman pumping (Fig. 7, upper panel). North of about 40°S, changes in the wind stress result in changes in wind stress curl, which in turn produce a positive Ekman pumping anomaly (i.e., less downward Ekman pumping compared to the CNTL simulation). As a result, a given isotherm is found at shallower depths (Fig. 7, lower panel). By contrast, south of about 40°S (but north of ~50°S, i.e., north of the latitudes where the wind stress curl changes sign) the Ekman pumping becomes more negative, contributing to a deepening of isotherms in the region (Fig. 7, lower panel). South of about 60°S upward Ekman pumping intensifies (Fig. 7, upper panel) resulting in increased upwelling of deep cold water, which in turn lifts the isotherms in the region (not shown).

Finally, we consider the UVic ESCM projected changes in the ACC. Working with the barotropic

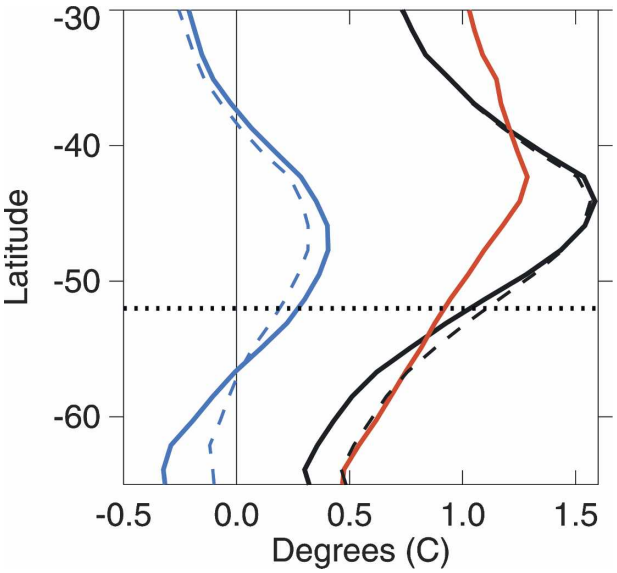

FIG. 6. UVic ESCM model simulations showing depth and zonally integrated ocean temperature change between 1850 and 2100 for the various experiments: (black) Both experiment; (red) GHG experiments; (blue) Wind experiment; (dashed black) BothE experiment; and (dashed blue) WindE experiment. Note that enhanced parameterized eddy activity leads to about a 25% increase in the warming south of 52°S. The horizontal dotted line denotes the mean position of the Antarctic Circumpolar Current.

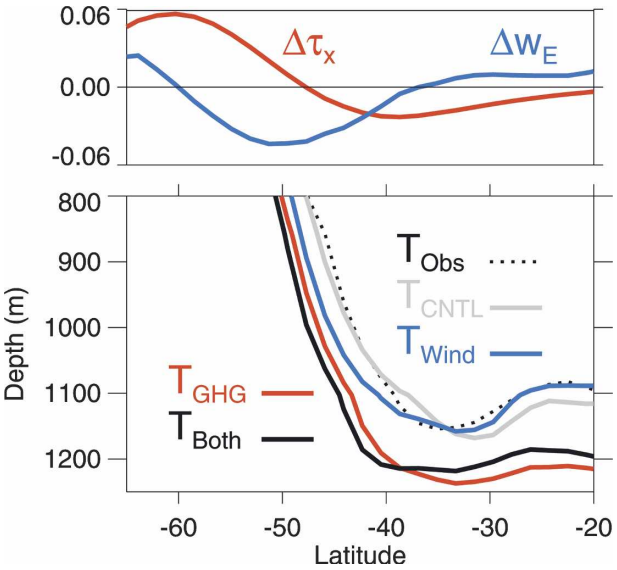

FIG. 7. UVic ESCM model simulations showing the dynamical influence of poleward intensification of annual-mean and zonal-mean ocean temperature: (top) 1850 to 2100 change in zonal surface wind stress, $\Delta\tau_x$ (in Pa), and Ekman pumping, Δw_E (in m s^{-1} $\times$ 10^{-5}); (bottom) 4°C isotherms at year 2100 for the Wind, GHG, and Both experiments, and for the present-day observations and CNTL experiment.

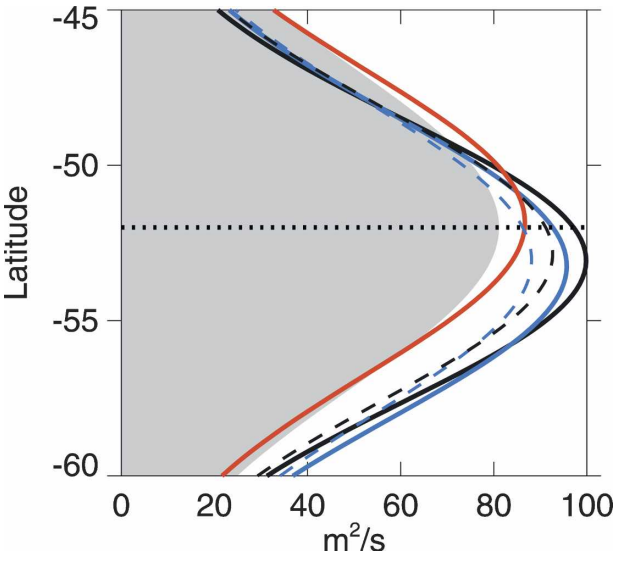

FIG. 8. UVic ESCM model simulations showing depth-integrated and along-axis-integrated Antarctic Circumpolar Current, $U(\phi)$, at year 2100 for the various experiments: (black) Both experiment; (red) GHG experiments; (blue) Wind experiment; (dashed black) BothE experiment; and (dashed blue) WindE experiment. The gray-shading represents the CNTL simulation with central latitude indicated with a dashed horizontal line.

streamfunction we follow a fitting procedure laid out in earlier work (Fyfe and Saenko 2006) to obtain an approximation for the depth-integrated and along-axis-integrated zonal current at a given time:

$$U(\phi) \sim \eta \exp\left[-\frac{(\phi - \Phi)^2}{\sigma^2}\right]. \quad (2)$$

In this way, the integrated zonal current can usefully be described in terms of its strength η (in units of m^2 s^{-1}), position Φ, and width σ. It also follows that the zonal transport by the ACC, T_U, is given by $T_U = R_e(\pi)^{1/2}\eta\sigma$, where R_e is the earth's radius. In this expression, we see that either strength or width changes are capable of producing changes in the net zonal transport, that is, $\Delta T_U/T_U \sim \Delta\eta/\eta + \Delta\sigma/\sigma$.

Figure 8 shows the ACC at year 2100 from the various experiments (see also Table 1, which shows the ACC parameter and transport values). We see that the poleward-intensified (and narrowed) ACC is largely due to poleward-intensified (and narrowed) winds, but there is a substantial contribution to the ACC strengthening from direct CO_2 emissions (i.e., accounting for about 30% of the strength increase). However, owing to changes in the width of the ACC, the zonal transport change directly due to CO_2 emissions is much less pronounced than the change in peak ACC velocity (i.e., the CO_2 emissions account for only about 5% of the

TABLE 1. Antarctic Circumpolar Current parameters of strength η, position Φ, width σ, and transport T_U at 2100.

Experiment	η ($m^2\ s^{-1}$)	Φ (°)	σ (°)	T_U (Sv; 1 Sv $\equiv 10^6\ m^3\ s^{-1}$)
CNTL	81.1	−52.0	7.4	117.8
Both	99.8	−53.1	6.4	126.8
GHG	86.7	−51.8	6.9	118.5
Wind	95.7	−53.2	6.9	130.6
BothE	92.6	−52.9	6.7	121.8
WindE	88.1	−53.1	7.1	124.0

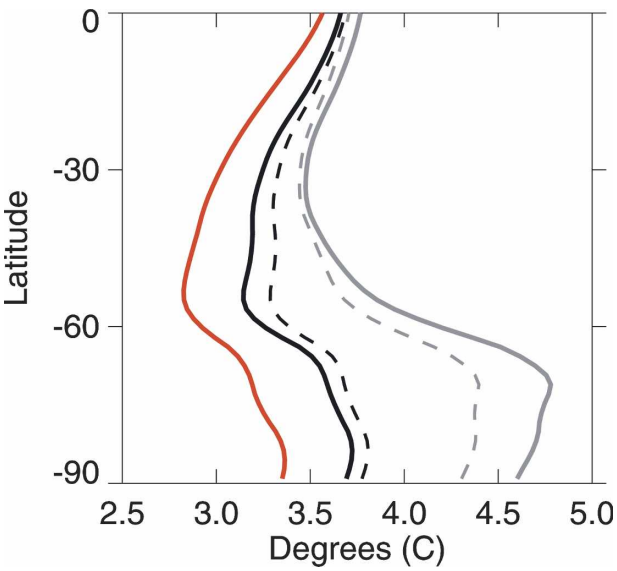

FIG. 9. UVic ESCM model simulations showing the zonally integrated surface air temperature change between 1950 and 2100 for the various experiments: (black) Both experiment; (red) GHG experiments; (gray) direct GHG-induced change added to the direct Wind-induced change; (dashed black) BothE experiment; and (dashed gray) direct GHG-induced change added to the direct WindE-induced change.

increase in zonal transport). Finally, we note that increased parameterized mesoscale eddy activity causes a substantial reduction in the increased ACC strength and zonal transport by year 2100. This supports some recent speculation that the inclusion of the effect of enhanced mesoscale eddy activity in relatively coarse-resolution climate models may produce different findings in terms of the projected increase in ACC transport (Meredith and Hogg 2006). Finally, we note that the ACC is presumably more bathymetrically constrained in reality than in our coarse-resolution model, and that there is some indication from eddy-resolving simulations that the real ACC transport may be eddy saturated (i.e., perhaps being less sensitive to changes in winds than coarse-resolution models would indicate). Further work with eddy-resolving models is clearly a matter of priority.

To conclude, we consider the surface air temperature change for the various UVic ESCM experiments (Fig. 9). We see that the time-varying surface winds result in increased surface air temperature in the Southern Hemisphere beyond that generated by the time-varying CO_2 emissions (comparing the solid black and red curves). At high latitudes, one reason for this appears to involve sea ice motion. The stronger westerly winds result in stronger offshore Ekman sea ice transport. This leads to enhanced regrowth of new sea ice in place of that transported from the coast of Antarctica, and the ice becomes, on average, thinner. The associated brine rejection and heat loss (including stronger conductive heat loss through the thinner ice) result in enhanced convection, cooling the deep ocean and warming the surface ocean and the atmosphere above (e.g., Saenko et al. 2002). In addition, the poleward-shifting zonal winds and ACC, with the warm air and water they bring in, tend to limit the northward expansion of the Southern Ocean sea ice during its growth season, thereby reducing the ice-covered area around Antarctica. In this regard, it is intriguing that the sum of the direct CO_2-induced warming (red curve) and the direct wind-induced warming is much greater than the warming from the Both experiment (comparing the gray and black curves). This is apparently the consequence of the CO_2 emissions leading to reduced sea ice (not shown). As a result, both the wind–ice–convection surface temperature mechanism, and also the mechanism whereby the sea ice cover is directly limited by the southward-shifting subpolar fronts, become less pronounced.

As for the case of enhanced mesoscale eddy activity we note the interesting situation whereby enhanced eddy activity dampens the surface warming when wind changes are in isolation (comparing the gray curves) and amplifies the warming when they are in combination (comparing the black curves). Our explanation for this begins with the recognition that the eddy-induced poleward heat transport tends both to directly melt sea ice (implying atmospheric warming) and to directly suppress convection (implying atmospheric cooling). Evidently, the balance between these opposing effects tips in favor of suppressed convection (leading to less atmospheric warming) when the winds act alone and reduced sea ice (leading to more atmospheric warming) when the winds act in combination. As a final remark, we note that the purpose here was only to illustrate the potential importance of the eddy feedback on the climate. More adequate parameterization(s) for *changing* mesoscale eddy activity in response to changing climate need to be incorporated into coarse-resolution climate

models. Once again, further work with eddy-resolving models is clearly a matter of priority.

4. Summary and discussion

We have explored the role that poleward-intensifying westerlies may have played in the higher than expected warming of the subsurface Southern Ocean observed since the 1950s. To this end a climate model of intermediate complexity was driven separately, and in combination, with time-varying CO_2 emissions and time-varying surface winds (derived from the latest series of fully coupled climate model simulations). The experiments have suggested that the combination of the direct radiative effect of CO_2 emissions and poleward-intensified winds sets the overall magnitude of Southern Ocean warming, and that the poleward-intensified winds are key in terms of determining its latitudinal structure (primarily through local changes in Ekman pumping). The experiments also support recent high-resolution ocean model experiments suggesting that enhanced mesoscale eddy activity associated with the poleward-intensified winds has influenced the subsurface warming. In particular, we found that increased poleward heat transport driven by increased mesoscale eddy activity enhances the subsurface warming south of the ACC. We have also reported on a mechanism involving offshore Ekman sea ice transport (modulated by enhanced mesoscale activity) that acts to significantly limit the human-induced high-latitude Southern Hemisphere surface temperature response. Overall, the results of the study will hopefully motivate further investigation involving models run with a more complete set of external forcings (e.g., volcanic aerosols and stratospheric ozone) and with explicitly resolved mesoscale eddies.

Acknowledgments. Comments from Charles Curry, Kos Zahariev, and an anonymous reviewer helped with the interpretation and presentation of the results. We acknowledge the international modeling groups for providing their data for analysis, the PCMDI for collecting and archiving the model data, the JSC/CLIVAR Working Group on Coupled Modelling (WGCM) and their Coupled Model Intercomparison Project (CMIP) and Climate Simulation Panel for organizing the model data analysis activity, and the IPCC WG1 TSU for technical support. The IPCC Data Archive at Lawrence Livermore National Laboratory is supported by the Office of Science, U.S. Department of Energy. This research was partially supported from grants provided from NSERC and CFCAS to the Canadian CLIVAR Network.

APPENDIX

Enhanced Parameterized Mesoscale Eddy Activity

The modification to the mesoscale eddy activity that we have prescribed in the UVic ESCM is based on the following considerations:

1) The net, or residual, overturning streamfunction in the upper Southern Ocean, Ψ_{res}, can be expressed as a sum of the meridional overturning due to the Eulerian mean flow, $\overline{\Psi}$, and that associated with mesoscale eddies, Ψ^*. We therefore can write (e.g., Marshall and Radko 2003) $\overline{\Psi}_{\text{res}} = \overline{\Psi} + \Psi^*$, where $\overline{\Psi}$ is associated with the northward Ekman flux, that is, $\overline{\Psi} = -\tau/(f\rho_o)$, with τ, f, and ρ_o being, respectively, the zonal-mean zonal wind stress, Coriolis parameter, and reference density of water. The eddy-induced overturning Ψ^* is associated with the eddy buoyancy fluxes. The Gent and McWilliams (1990) approach assumes that the eddy buoyancy fluxes are "adiabatic" in the interior (i.e., they follow mean isopycnals), so that $\Psi^* = \kappa s_\rho$, where s_ρ represents the slope of the isopycnals. Under these assumptions, the residual overturning streamfunction is given by

$$\Psi_{\text{res}} = -\frac{\tau}{f\rho_o} + \kappa s_\rho. \tag{A1}$$

2) High-resolution ocean modeling experiments (Hallberg and Gnanadesikan 2006) suggest that the residual overturning streamfunction responds only weakly in steady-state to positive zonal wind stress anomalies within the ACC. Therefore, under slowly increasing wind stress (i.e., nearly steady conditions) we write

$$-\frac{\tau(0)}{f\rho_o} + \kappa(0)s_\rho \approx -\frac{\tau(t)}{f\rho_o} + \kappa(t)s_\rho, \tag{A2}$$

where $\tau(0)$ and $\kappa(0)$ are year 1850 values.

3) The high-resolution ocean modeling experiments (Hallberg and Gnanadesikan 2006) also suggest that the slope of the isopycnals across the ACC responds only weakly to positive zonal wind stress anomalies. From this result and (A2) we get

$$\Delta\kappa = \alpha\Delta\tau, \tag{A3}$$

where $\Delta\kappa = \kappa(t) - \kappa(0)$, $\Delta\tau = \tau(t) - \tau(0)$, and $\alpha = (f\rho_o s_\rho)^{-1}$. Here we set $\alpha = \kappa(0)/\tau(0)$. We represent the direct mesoscale eddy response to poleward-intensified winds in this simple way, which nevertheless aims to plausibly capture the relevant processes. Our purpose here is to test the role of enhanced mesoscale eddy activity in the context of the Gent

and McWilliams parameterization as implemented in most coarse-resolution models.

REFERENCES

Cox, P. M., 2001: Description of TRIFFID dynamic global vegetation model. Hadley Centre Tech. Note 24, 32 pp.

——, C. Huntingford, and R. J. Harding, 1998: A canopy conductance and photosynthesis model for use in a GCM land surface scheme. *J. Hydrol.,* **212–213,** 79–94.

Fyfe, J. C., 2006: Southern Ocean warming due to human influence. *Geophys. Res. Lett.,* **33,** L19701, doi:10.1029/2006GL027247.

——, and O. A. Saenko, 2006: Simulated changes in extratropical Southern Hemisphere winds and currents. *Geophys. Res. Lett.,* **33,** L06701, doi:10.1029/2005GL025332.

Gent, P. R., and J. C. McWilliams, 1990: Isopycnal mixing in ocean general circulation models. *J. Phys. Oceanogr.,* **20,** 150–155.

Gille, S., 2002: Warming of the Southern Ocean since the 1950s. *Science,* **295,** 1275–1277.

Gillett, N. P., and D. W. Thompson, 2003: Simulation of recent Southern Hemisphere climate change. *Science,* **302,** 273–275.

Hallberg, R., and A. Gnanadesikan, 2006: The role of eddies in determining the structure and response of the wind-driven Southern Hemisphere overturning: Results from the modeling eddies in the Southern Ocean project. *J. Phys. Oceanogr.,* **36,** 2232–2252.

Kamenkovich, I. V., and E. S. Sarachik, 2004: Mechanisms controlling the sensitivity of the Atlantic thermohaline circulation to the parameterization of eddy transports in ocean GCMs. *J. Phys. Oceanogr.,* **34,** 1628–1647.

Kushner, P. J., I. M. Held, and T. L. Delworth, 2001: Southern Hemisphere atmospheric circulation response to global warming. *J. Climate,* **14,** 2238–2249.

Levitus, S., J. I. Antonov, T. P. Boyer, 2005: Warming of the World Ocean, 1955–2003. *Geophys. Res. Lett.,* **32,** L02604, doi:10.1029/2004GL021592.

Marshall, G. J., 2003: Trends in the southern annular mode from observations and reanalyses. *J. Climate,* **16,** 4134–4143.

Marshall, J., and T. Radko, 2003: Residual-mean solutions for the Antarctic Circumpolar Current and its associated overturning circulation. *J. Phys. Oceanogr.,* **33,** 2341–2354.

Matthews, H. D., A. J. Weaver, K. J. Meissner, N. P. Gillett, and M. Eby, 2004: Natural and anthropogenic climate change: Incorporating historical land cover change, vegetation dynamics and the global carbon cycle. *Climate Dyn.,* **22,** 461–479.

Meissner, K. J., A. J. Weaver, H. D. Matthews, and P. M. Cox, 2003: The role of land-surface dynamics in glacial inception: A study with the UVic Earth System Model. *Climate Dyn.,* **21,** 515–537.

Meredith, M. P., and A. M. Hogg, 2006: Circumpolar response of Southern Ocean eddy activity to a change in the southern annular mode. *Geophys. Res. Lett.,* **33,** L16608, doi:10.1029/2006GL026499.

Oke, P. R., and M. H. England, 2004: Oceanic response to changes in the latitude of the Southern Hemisphere subpolar westerly winds. *J. Climate,* **17,** 1040–1054.

Russell, J. L., R. J. Stouffer, and K. W. Dixon, 2006: Intercomparison of the Southern Ocean circulations in the IPCC coupled model control simulations. *J. Climate,* **19,** 4560–4575.

Saenko, O. A., A. Schmittner, and A. J. Weaver, 2002: On the role of wind-driven sea ice motion on ocean ventilation. *J. Phys. Oceanogr.,* **32,** 3376–3395.

Schmittner, A., A. Oschlies, X. Giraud, M. Eby, and H. L. Simmons, 2005: A global model of the marine ecosystem for long term simulations: Sensitivity to ocean mixing, buoyancy forcing, particle sinking and dissolved organic matter cycling. *Global Biogeochem. Cycles,* **19,** GB3004, doi:10.1029/2004GB002283.

Thompson, D. W. J., J. M. Wallace, and G. C. Hegerl, 2000: Annular modes in the extratropical circulation. Part II: Trends. *J. Climate,* **13,** 1018–1036.

Weaver, A. J., and Coauthors, 2001: The UVic Earth System Climate Model: Model description, climatology and application to past, present and future climates. *Atmos.–Ocean,* **39,** 361–428.

Yin, J. H., 2005: A consistent poleward shift of the storm tracks in simulations of 21st century climate. *Geophys. Res. Lett.,* **32,** L18701, doi:10.1029/2005GL023684.

Zickfeld, K., J. C. Fyfe, O. A. Saenko, M. Eby, and A. J. Weaver, 2007: Response of the global carbon cycle to human-induced changes in the Southern Hemisphere winds. *Geophys. Res. Lett.,* **34,** L12712, doi:10.1029/2006GL028797.